High-Resolution Spectroscopy of Methyl 4-Hydroxycinnamate and Its Hydrogen-Bonded Water Complex

Mattijs de Groot,[†] Evgeniy V. Gromov,[‡,§] Horst Köppel,[‡] and Wybren Jan Buma*[,†]

Van't Hoff Institute for Molecular Sciences, Faculty of Science, University of Amsterdam, Nieuwe Achtergracht 166, 1018 WV Amsterdam, The Netherlands, Theoretische Chemie, Physikalisch-Chemisches Institut, Universität Heidelberg, Im Neuenheimer Feld 229, D-69120 Heidelberg, Germany, and Laboratory of Quantum Chemistry, Computer Center, Irkutsk State University, K. Marks 1, 664003 Irkutsk, Russian Federation

Received: October 18, 2007; In Final Form: December 12, 2007

The electronic structure and spectroscopic properties of the lower excited singlet states of methyl 4-hydroxycinnamate, a model for the chromophore of the photoactive yellow protein in neutral form, have been investigated using various high-resolution gas-phase spectroscopic techniques and quantum-chemical calculations. The experiments show that under our experimental conditions the molecule can adopt four conformations with similar spectroscopic properties. From the detailed assignment of the vibrationally active modes in excitation and emission spectra, it is concluded that the S_1 and S_2 states should be assigned to the V′ and V $\pi\pi^*$ states that are characterized by, respectively, small and large contributions of the HOMO → LUMO excitation. We find that complexation with a single water molecule affects the spectroscopic properties of methyl 4-hydroxycinnamate considerably in terms of stabilization of the lowest excited singlet state but in particular with respect to the transition intensities. The latter observation is tentatively interpreted as being caused by an increase in the oscillator strength of the respective electronic transition as well as by a rise/removal of conical intersections with the $\pi\sigma^*$ state.

Introduction

The excited-state properties of *p*-coumaric acid (pCA), the chromophore of the photoactive yellow protein (PYP), have been the subject of a large number of studies. For a recent overview of the biochemistry of PYP, see for example ref 1. In some studies the chromophore *in vacuo*, either in its deprotonated[2,3] or in its neutral[4] form, was used as a model for the actual chromophore in the protein. This is of interest to help ascertain the role of the protein environment in the initial trans-to-cis isomerization that takes place at the start of the photocycle.[5] The results of such studies can be directly compared with predictions of the quantum-chemical calculations that, in turn, can give detailed information on the excited-state dynamics of the chromophore. Recently we showed using mass-resolved resonance-enhanced multiphoton ionization (MR-REMPI) experiments that the species actually giving rise to the laser-induced fluorescence (LIF) spectra in the first gas-phase study on neutral pCA[4] was *p*-vinylphenol (pVP) formed by thermal decarboxylation in the oven prior to expansion in the supersonic jet.[6] This implies that, as yet, no high-resolution experimental data is available on the neutral form of the chromophore of PYP in the gas phase.

In a previous paper we have reported vibrationally resolved spectra and their interpretation for pVP, which can be viewed as a minimal model chromophore of PYP.[7] Here, we will go several steps further and consider a model chromophore that includes an ester moiety similar to that present in the protein. Because in the actual protein the pCA chromophore is linked to the backbone *via* a thioester bond and the substitution of oxygen by sulfur appears to have a large effect on the energetics of the chromophore,[8] the most natural chromophore to study in the gas phase in connection with the PYP photoactive cycle would be the methylthio ester of pCA (TMpCA). This molecule has, however, turned out to remain elusive in preliminary high-resolution LIF and REMPI experiments.[9] The subject of the current study is therefore the methyloxy ester of pCA (OMpCA) (Figure 1). Under real-life conditions the pCA chromophore in PYP is subject to interactions with its environment. As a first step to mimic and investigate the influence of such interactions, we have studied OMpCA as well under microsolvation conditions in which the chromophore is complexed with a single water molecule that acts as a hydrogen bond acceptor for the phenolic OH group.

A specific question we would like to answer with the current study pertains to the ordering of the two lower excited singlet states in the Franck−Condon region. In our pVP study we showed that it is complicated to obtain a correct description of the two lower $\pi\pi^*$ states of this molecule with TD-DFT. Assuming that the EOM-CCSD results from that study are correct, which seems likely considering the excellent agreement with the experimental results, the S_1 state has a small HOMO → LUMO contribution and a small oscillator strength, while the S_2 state has a large HOMO → LUMO contribution and a large oscillator strength. In the following we will label the states with small and large oscillator strength as V′ and V, respectively. The successful description of these state characteristics with TD-DFT was shown to depend sensitively on the choice of the exchange correlation functional employed in the calculations. We concluded that the BP86 functional yields the best descrip-

* Author to whom correspondence should be addressed.
[†] University of Amsterdam.
[‡] Universität Heidelberg.
[§] Irkutsk State University.

10.1021/jp7101308 CCC: $40.75
Published on Web 03/14/2008

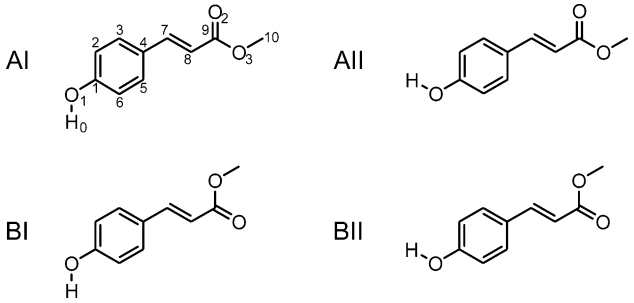

Figure 1. Structure of methyl 4-hydroxycinnamate (OMpCA) and atom labeling employed. Indicated are the four conformations of importance to the present study: AI (s-cis, OH syn), AII (s-cis, OH anti), BI (s-trans, OH syn), and BII (s-trans, OH anti).

tion of the S_1 and S_2 states in the case of pVP, and that a study of the functional dependence and a calibration with EOM-CCSD results was essential for the successful application of TD-DFT on the analogous states of similar molecules.

Gromov et al.[8] showed that the two lower $\pi\pi^*$ states of pCA calculated with EOM-CCSD exhibit characteristics similar to those of pVP, albeit with a smaller V′−V gap. They demonstrated that the V′ and V states mix substantially and have complex electronic structure, with the V state having some charge-transfer character.[8,10] It was concluded that low-correlation methods, in particular CIS and partly CC2, poorly describe these states, which in the case of CIS results in their wrong ordering.[8] Ko et al.[11] used state-averaged CAS-SCF and CASPT2 calculations to study excited-state dynamics of pCA and later compared those calculations to results obtained with TD-DFT.[12] In the light of the above discussion, the nearly quantitative agreement that was found between CASPT2 and TD-DFT results is worrying and might also indicate that the CAS-SCF and CASPT2 calculations of Ko et al. lead to an incorrect state ordering. We emphasize that for a qualitative description of the excited-state dynamics (e.g., photoisomerization) the correct prediction of the shape of the potential energy surface is more important than the excitation energy. However, when excited-state crossings are involved in the dynamics, the correct ordering of the states is, of course, essential. In the present study, we have extended the CAS-SCF calculations by calculating the oscillator strengths of the relevant transitions, and we have compared these calculations with experimental results as well as EOM-CCSD calculations in order to establish the proper excited-state ordering.

Apart from investigating the effect of the carboxylic ester group on the ordering of the lower excited states, the present study also aims to explore how the increased conformational freedom influences the spectroscopic properties of these states. To this purpose, we will in the following present REMPI, LIF, and UV−UV hole-burning spectra, assign those spectra to various conformers of the bare molecule and its complex with one water molecule, and interpret them based on the theoretical predictions by EOM-CCSD and TD-DFT calculations.

Experimental and Theoretical Details

Experimental Procedures. In both REMPI and LIF experiments the molecular expansion was created with the same injector assembly that consisted of a stainless-steel oven in which a glass container with the sample was placed and kept at a temperature of 160 °C. The oven was connected to a pulsed valve (General Valve) with a nozzle diameter of 0.5 mm that was typically kept 10 °C above the oven temperature to prevent clogging of the nozzle. Helium at the desired backing pressure of 1.5−4 bar was led through the oven and expanded through the nozzle into the vacuum chamber.

For the REMPI experiments, the skimmed molecular beam was crossed with the frequency-doubled (BBO) output of a Sirah Precision Scan dye laser operating on either DCM or a mixture of Rhodamine 610 and 590 dyes and pumped by the frequency-doubled output of a Nd:YAG laser (Spectra Physics Lab 190). Mass-resolved ion detection was achieved with a reflectron time-of-flight spectrometer (R.M. Jordan Co.) that was calibrated by adding a small amount of pyrazine to the expansion.

For the LIF experiments the unskimmed jet was crossed with the frequency-doubled (KDP or BBO) beam from a dye laser (Lumonics HD300). The dye laser was pumped with 308 nm from a XeCl excimer laser (Lumonics HyperEx 400). Details of this setup have been reported elsewhere[13] albeit that for the current experiments an ARC SpectraPro-500i monochromator was employed.

For the hole-burning spectra, a second dye laser (Lumonics HD300) was used that was pumped by the same excimer laser *via* a 50% beam splitter. An optical delay of ca. 18 m was used to introduce a delay of 60 ns between pump and probe pulses. A fast photomultiplier (Philips XP 2254B) was connected to a digitizing oscilloscope (Tektronix TDS 684B). The signal from the photomultiplier was averaged on the scope for 60 samples and subsequently processed by a PC. The wavelength of the hole-burning laser was set to the maximum of the peak of interest, and the probe laser was scanned. A shutter was used to record a signal with and without the hole-burning laser at all wavelengths of the probe laser. The hole-burning spectra reported in this paper were constructed by subtracting the signal with the hole-burning laser from the signal without the hole-burning laser.

Theoretical Procedures. Density functional calculations were performed using the TURBOMOLE 5.7 suite of programs[14−17] analogous to our previous calculations on phenol, styrene, and pVP.[7,18,19] Various functionals were tested (BP86[20,21] and the hybrid functionals B3LYP[21−23] and BHLYP[21,23,24]). In contrast to the results obtained for pVP, all functionals gave similar results for geometries as well as force fields. In the following we will therefore only report the results obtained with the most commonly applied B3LYP functional. A Gaussian basis set of triple-ζ quality augmented with polarization functions (def-TZVP) was used throughout. Frequencies calculated with this functional were scaled with a factor of 0.96.[25] For the calculation of vibronic spectra, we used an in-house developed program[26] that is based on the recursion relations for Franck−Condon integrals.[27] Reconstruction of the excited-state equilibrium geometry from the experimental intensities of the $\nu_i(a')_1^0$ transitions was performed using the procedures described by Doktorov.[28]

Apart from TD-DFT calculations, we performed CAS-SCF calculations of vertical excitation energies and oscillator strengths using GAMESS.[29,30] For the CAS-SCF calculations on pCA, the geometry was taken from the Supporting Information supplied by Ko et al. in order to facilitate comparison to their values. After selection of the proper orbitals for inclusion in the active space, excitation energies were calculated using a three- or five-state-averaged CAS-SCF calculation (SA3 or SA5) with six electrons in five active orbitals and a 6-31G* basis set, analogous to the calculations of Ko et al. Subsequently, the optimized state-averaged CAS-SCF orbitals were used to calculate the oscillator strengths using a CAS-CI expansion of the ground and excited states.

TABLE 1: Calculated Vertical Excitation Energies (eV) and, in Parentheses, the Oscillator Strengths for pCA, OMpCA, and OMpCA(H_2O)

	pCA			OMpCA			OMpCA(H_2O)
state	TD-DFT	CAS-SCF[a]	EOM-CCSD[b]	TD-DFT	CAS-SCF[a]	EOM-CCSD	EOM-CCSD
S_1 ($\pi\pi^*$)	4.15 (0.64)	SA3: 5.57 (0.04) SA5: 5.67 (0.75)	4.69 (0.16)	4.16 (0.69)	SA3: 5.64 (0.03) SA5: 5.77 (0.75)	4.69 (0.13)	4.63 (0.25)
S_2 ($\pi\pi^*$)	4.58 (0.02)	SA3: 6.25 (0.79) SA5: 6.08 (0.42)	4.95 (0.61)	4.59 (0.03)	SA3: 6.32 (0.80) SA5: 6.13 (0.42)	4.99 (0.67)	4.87 (0.57)
S_3 ($n\pi^*$)			5.27 ($<10^{-3}$)			5.28 ($<10^{-3}$)	5.31 ($<10^{-3}$)
S_4 ($\pi\sigma^*$,Ryd)			5.67 ($<10^{-3}$)			5.61 ($<10^{-3}$)	5.75 ($<10^{-3}$)

[a] CAS-SCF (6/5) results using state-averaged orbitals. State averaging over the lowest three (SA3) and five (SA5) states. [b] The results differ from the values of ref 8 because of the diffuse functions in the basis set used in the present study. The S_1-S_3 states are only slightly affected (they are valence states) while the S_4 state is not described correctly when disregarding the diffuse functions (its energy increases by ca. 2 eV) because of substantial Rydberg character of this state.[7]

The results of the TDDFT and CAS-SCF calculations are verified against predictions of the more accurate (although more computationally expensive) coupled-cluster singles and doubles (EOM-CCSD) method.[31] The characteristics and performance of the method are described/shown in our previous studies of refs 7 and 8. The present EOM-CCSD results were obtained using the MOLPRO 2006 set of programs[32] where a parallel version of the EOM-CCSD method is available. The 6-31+G* basis set, holding polarization *and* diffuse functions, was employed, providing a correct description of the state ($\pi\sigma^*$) with substantial Rydberg character. All EOM-CCSD calculations were performed at the ground-state equilibrium geometries, obtained with the conventional CCSD method and the 6-31G* basis set. The core orbitals were kept frozen in the CCSD and EOM-CCSD calculations.

Results and Discussion

Although the main focus of this article will be on the experimental results obtained for OMpCA, it will be advantageous for the flow of the text to start with a brief description of the theoretical results. We will then discuss the experimental data in the light of the theoretical predictions.

Theoretical Results. *The Lowest $\pi\pi^*$ States.* In Table 1 we compare the vertical excitation energies and oscillator strengths of the two lower $\pi\pi^*$ states of pCA and OMpCA calculated with TD-DFT, state-averaged CAS-SCF, and EOM-CCSD. The CAS-SCF excitation energies for pCA are identical to the results reported by Ko et al. with the exception of the value for the S_2 state in the SA3 calculation that is probably a typo in Table 1 of ref 11. While EOM-CCSD finds S_1 to be the V′ state (smaller oscillator strength) for both molecules, TD-DFT and SA5-CAS-SCF, the methods used by Ko et al. to calculate the potential energy surface of pCA predict that S_1 is the V state (larger oscillator strength) for pCA and OMpCA. Table 1 clearly shows that the CAS-SCF calculations are very sensitive to the state-averaging procedure. When only the excitation energies are compared, it might appear as if the SA3- and SA5-CAS-SCF give very similar results, but this is rather misleading; inspection of the oscillator strengths reveals that the character of the states is completely different in the two calculations. A similar conclusion is reached by a detailed inspection of the CI vectors of the relevant states in the Supporting Information of ref 11 as well as in our current calculations: the S_1 state in the SA5 calculation contains a larger HOMO → LUMO contribution than the S_2 state. The SA3-CAS-SCF calculations predict the same characteristics for the states as EOM-CCSD. It would thus appear that the calculations of the excited-state dynamics of pCA[11] were not done with the appropriate potential energy surfaces.

Comparison of the EOM-CCSD results for pCA and OMpCA (Table 1) indicates that the influence of the methyl substituent is very small. In addition, we performed geometry optimization of the excited states of OMpCA using the EOM-CCSD method (unpublished results) which reveals further similarities between OMpCA and pCA. In particular, the in-plane stationary points of the excited states in these molecules are almost identical regarding their energetics and structural parameters. The latter suggests that our predictions on pCA in ref 8 (particularly in Figure 2 of ref 8) can be transferred to the case of OMpCA. Note, that the current EOM-CCSD vertical excitation energies for pCA are somewhat lower than those reported in refs 8 and 11. This is due to the inclusion of diffuse functions in the basis set used for the current calculations. As mentioned before, these functions are absolutely necessary for a proper description of the $\pi\sigma^*$ state (see below), but they also slightly affect the other states under consideration.

Note on the Higher-Lying States. Table 1 also displays our EOM-CCSD results for the next two excited states of pCA and OMpCA, which are $n\pi^*$ and $\pi\sigma^*$ in order of increasing transition energy. Despite the higher vertical excitation energies and very low oscillator strengths, these states might have an influence on the low-energy photophysics and photochemistry of the molecules under consideration and related compounds. This follows from the fact that, upon relaxation, both states experience a substantial energy lowering and become the lowest excited state (S_1) at their respective equilibrium geometries.[33] More specifically, the $n\pi^*$ state is S_1 at its in-plane equilibrium structure (see Figure 2 in ref 8), while the $\pi\sigma^*$ state is predicted to be unbound with respect to the abstraction of the phenolic hydrogen, based on our findings for pVP (see Figure 5 in ref 7) and the previous studies on phenol.[34] Both states are expected to be involved in nonradiative decays after transitions to the $\pi\pi^*$ states (see below).

Experimental Results

Gas-Phase Spectra. Figure 2 displays the laser-induced fluorescence spectrum of OMpCA. MR-REMPI experiments show that all peaks in the spectrum derive from a species with a molecular mass of 178 amu, the mass of OMpCA. Before we can interpret the spectrum in terms of structural changes of OMpCA in the excited state, we need to establish which peaks belong to each of the possible conformations of OMpCA. In total we can expect four conformations with energies low enough to be present under the conditions in the oven prior to the expansion; all of these conformations can be "frozen in" by cooling in the expansion: the phenolic OH group can be in either the syn- or the anti-position with respect to the vinylic $C_7{=}C_8$ double bond (for labeling scheme, see Figure 1).

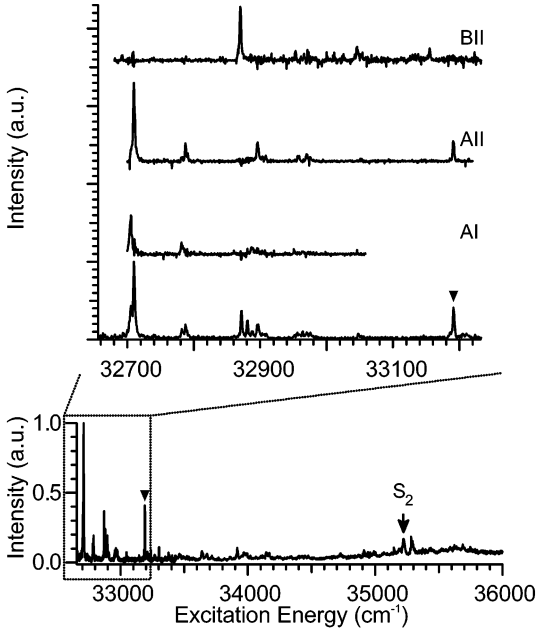

Figure 2. Bottom: LIF excitation spectrum of OMpCA. The triangle (▼) marks a prominent band missing from the simulated spectrum (Figure 3 (bottom)). At 35220 cm^{-1} the S_2 origin is marked in the spectrum. Top: the inset displays a zoom-in of the low-energy region of the spectrum (bottom spectrum of the inset) and hole-burning spectra of three of the four conformations that are expected to contribute to the spectra. The hole-burning laser was fixed at 32705, 32710, and 32871 cm^{-1} for the spectra of AI, AII, and BII conformers respectively. The origin of the BI conformer presumably lies at 32868 cm^{-1}, but because of its low-intensity we are not able to confirm this conclusion by hole-burning spectroscopy.

Likewise, the C_9═O bond can be oriented either cis or trans around the C_8-C_9 single bond with respect to the C_7═C_8 double bond. The four conformations and labels used are depicted in Figure 1.

Both DFT and CCSD calculations predict that the s-cis conformations (A) have a lower energy than the s-trans (B) conformations (0.9 and 1.0 kcal/mol for DFT and CCSD calculations, respectively). This energy difference leads to the prediction that about 30% of the molecules will be in the B conformation at 170 °C. For the OH syn (I) and anti (II) conformations, one would expect a much smaller energy difference and only minor effects on the vibronic spectra. Indeed, with both DFT and CCSD, conformer II is predicted to be the lowest energy conformer (but only by 0.1 kcal/mol), in agreement with the results previously obtained for pVP.[7]

Hole-burning spectra with the burn laser fixed at 32705 or 32710 cm^{-1} are shown in the inset of Figure 2. The spectra clearly show that these peaks belong to two different species with only slightly shifted spectra. We assign those peaks to the origin bands of the AI and AII conformers, respectively. The intensity ratio of the peaks ($I_{AI}/I_{AII} = 0.43$) is, however, much smaller than expected from the calculated energy difference. Vice versa, if we assume that the peak intensities represent the equilibrium distribution between I and II conformers in the oven at a temperature of 170 °C, we find an energy difference of 0.7 kcal/mol, which on chemical grounds would seem much too high. We recall that also for pVP an energy difference of ~0.1 kcal/mol was calculated for the syn and anti conformers, and that in that case indeed a ratio much closer to 1 was found, in agreement with the expected Boltzmann distribution at the experimental conditions.[7]

We conclude from these observations that in the electronic ground state the barrier for interconversion between the syn and anti conformers is lower in OMpCA than in pVP. If the barrier is low enough to allow the conformers to stay at thermodynamic equilibrium during the cooling process in the jet, the intensity ratio will reflect the temperature at which the conformations decouple and the distribution freezes in. Using the theoretically predicted ΔE of 0.1 kcal/mol and the experimentally observed ratio of 0.43, our results imply that this decoupling occurs at 60 K. At first sight there does not seem to be a simple explanation for the observed difference in barrier height between OMpCA and pVP.

The strong peak at 32871 cm^{-1} does not appear in either one of the hole-burning spectra corresponding to conformations AI and AII. When a hole-burning laser is set to this peak, we find that the band corresponds to a species that displays a blue shift of 161 cm^{-1} with respect to conformer AII. On the basis of the lower intensity of this peak, we assign it to the origin of the s-trans species BII. It is reasonable to assign a small peak that appears in the spectrum at 32868 cm^{-1} to the corresponding origin of the BI conformer, but because of its very low-intensity we are not able to confirm this conclusion by the hole-burning spectrum for that species.

The magnitude of the fluorescence dips is more than 50% for most peaks, indicating that rapid depopulation of the state excited by the hole-burning laser occurs on a time scale faster than the width of the laser pulse (i.e., <10 ns). This is not surprising as there are two obvious nonradiative decay pathways from the S_1 state. First, there is the $n\pi^*$ state that is, adiabatically, the lowest energy state (*vide supra*). According to ref 8, conical intersections between the $n\pi^*$ and $\pi\pi^*$ states should be expected, which provide efficient pathways for internal conversion from the $\pi\pi^*$ to the $n\pi^*$ state (to provide more precise insight into the involvement of the $n\pi^*$ and its coupling with the $\pi\pi^*$ states, further theoretical investigations are needed). Second, the $\pi\sigma^*$ state that plays an important role in the nonradiative decay in phenol[34,35] could also be involved. In the latter case, again conical intersections, involving first $\pi\pi^*$ and $\pi\sigma^*$ and then $\pi\sigma^*$ and the ground state, are crucial for the nonradiative decay (*vide infra*).

The assignment of all major features of the spectrum to one of the possible conformers allows us to interpret the spectra in terms of being associated with either the V′ or with the V state. Figure 3 displays Franck−Condon simulations based on the TD-DFT/B3LYP S_0, S_1, and S_2 geometries and force fields. The major feature that distinguishes the S_1 and S_2 excitation spectra in Figure 3 is the much stronger activity of the lowest energy a′ mode in the S_1 spectrum. This intramolecular bending mode, that we will label a'_1, was found to be very active in the S_2 (rather than S_1) spectra of both pVP[7] and styrene,[18] which is associated with the excited-state of V character. Extension of the molecule with an ester group leads to a much lower frequency, 81 cm^{-1} for OMpCA versus 220 and 244 cm^{-1} for pVP and styrene, respectively, but it is essentially the same mode. Because the activity of a'_1 in the experimental spectrum of OMpCA in Figure 2 is quite low and in much better agreement with the simulated S_2 spectrum (Figure 3 (bottom)), it is reasonable to assign this part of spectrum to the V′ state (in agreement with the assignment of the S_2 state calculated with TD-DFT to V′ [see discussion above and Table 1]). We thus conclude that for OMpCA the EOM-CCSD state ordering is correct and that TD-DFT incorrectly places the V state below the V′ state. The same situation is likely to hold true for pCA.

Because the LIF signals for OMpCA are much smaller than for pVP, we have not been able to measure a dispersed emission spectrum with a sufficiently high signal-to-noise ratio to allow

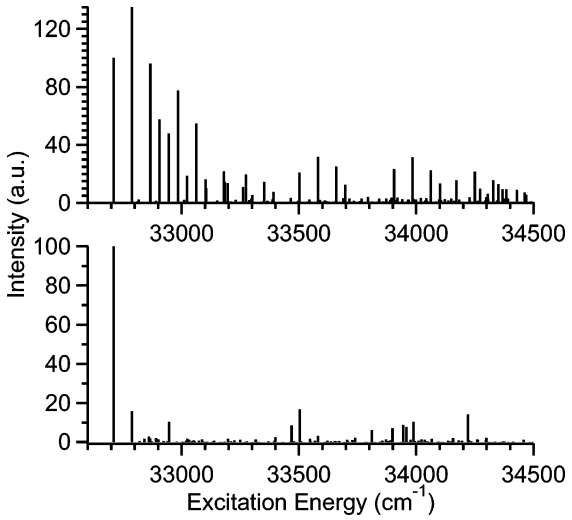

Figure 3. Franck−Condon simulations of the excitation spectrum calculated at the TD-DFT/B3LYP level. Top: based on geometries and force fields of S_0 and S_1. Bottom: based on geometries and force fields of S_0 and S_2. For both spectra the origin has been offset to 32710 cm^{-1} to allow for a comparison with the experimental excitation spectrum.

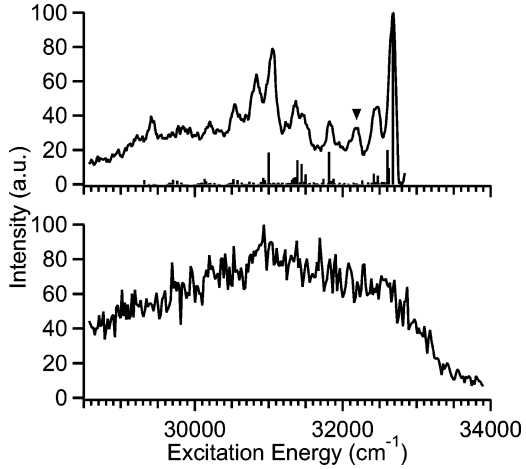

Figure 4. Top: dispersed emission spectrum obtained after excitation of the 0^0 level of S_1 of OMpCA (solid line) and Franck−Condon simulation (stick spectrum). The triangle (▼) marks a prominent band missing from the simulated spectrum. Bottom: dispersed emission spectrum obtained after excitation of the 0^0 level of S_2 of OMpCA. Because of the low signal strength, very wide slits were used for the latter spectrum.

for a line-by-line comparison with the theoretically predicted spectrum as has been done for pVP. A comparison of the simulated spectrum with an emission spectrum at lower resolution (Figure 4) shows, however, that the general shape of the spectrum is simulated fairly accurately and supports the conclusion drawn on the character of the excited state from the excitation spectra. One band that is notably absent from the predicted spectrum is the band at 32200 (510 cm^{-1}) marked with a triangle (▼). We note that the corresponding peak in the excitation spectrum of Figure 2 at 33191 (482 cm^{-1}), also marked, is likewise missing from the simulated spectrum. The fact that it is present in both excitation and emission spectra indicates that it must be assigned to a fundamental of an a′ mode. It can be either ν_{22} or ν_{23}, which both have suitable frequencies (514 and 532 cm^{-1}, respectively). On the other hand, our preliminary calculations with the EOM-CCSD/LVC approach, used in the study of pVP,[7] predict strong activity of mode ν_{25} (874 cm^{-1} in the ground state). The latter mode is similar in character to mode ν_7, found to be strongly excited in the $S_0 \leftrightarrow S_1$ spectra of pVP (see Figures 2 and 7 in ref 7). Nevertheless, the big difference in the frequency of ν_{25}, compared with the value observed in the emission spectrum (510 cm^{-1}), is puzzling and requires further clarification.

The assignment of S_1 to the V′ state suggests that evidence for the S_2 (V) state with a strong activity of mode a'_1 might be found at higher excitation energies. Indeed, at 35220 cm^{-1} in the LIF spectrum of Figure 2 a band is present that we assign to the origin transition to the V state. Because (i) no fundamentals with an energy close to 2510 cm^{-1} exist in OMpCA and (ii) there are no obvious candidates for overtones or combination modes with such a large intensity at this energy, an assignment to a vibrational band of S_1 is unlikely. Furthermore, the band at 35290 cm^{-1} can be very well assigned to the $(a'_1)^1_0$ transition to the V state.

Hole-burning experiments prove that these bands arise from the same species that is responsible for the band at 32710 cm^{-1}. The width of the bands in this region of the spectrum is much larger than at the V′ origin. Most likely this is caused by a very short lifetime of the S_2 state; the observed line width of approximately 20 cm^{-1} suggests a lifetime of approximately 250 fs. An emission spectrum recorded after excition at 35220 cm^{-1} (Figure 4 (bottom)) shows a broad band centered around 30800 cm^{-1} corresponding to emission from a large ensemble of a vibrational states of the V′ state populated after internal conversion from the V state.

All experimental results considered, it can be concluded that the general characteristics of the lower excited states in the Franck−Condon region of OMpCA closely resemble those of pVP discussed previously. Even though the ordering of the two lower singlet states calculated with TD-DFT is not correct for all tested functionals, the main structural characteristics of the states are described quite accurately.

H_2O Cluster. Starting at 32069 cm^{-1}, red-shifted from the AII origin by 641 cm^{-1}, some very strong signals appear that are very sensitive to the backing pressure and the timing of the molecular beam. This region of the spectrum is shown in Figure 5. MR-REMPI experiments show that those bands belong to a species with a molecular weight of 196 amu. The combination of mass and observed dependence on experimental conditions strongly suggest that this species is a hydrogen-bonded cluster of OMpCA with a single water molecule. Because of the high acidity expected for the phenolic OH group in OMpCA, the most likely structure for the cluster is the structure depicted in Figure 5, where water acts as a hydrogen bond acceptor to the phenolic OH group.[36] The red shift observed in the excitation spectrum is a well-known effect generally ascribed to the large increase of the acidity that occurs upon excitation of aromatic alcohols (see for examples, ref 37), but in the present case it seems exceptionally large.

Another striking feature of the water cluster peaks is their intensity; even at low backing pressures (when cluster formation is less than optimal) the intensity is much larger than the intensity of the peaks from the bare molecule. Comparing the strongest peak of Figure 5 with the origin peak of the bare molecule (marked with an asterisk), it is clear that the fluorescence intensity increases by more than a factor of 10. Because it seems unlikely that the abundance of the complex in the jet is larger than that of the bare molecule, the increased fluorescence signal can either be caused by an increase of the oscillator strength or by a decrease of the nonradiative decay rate.

A possible mechanism for a direct increase of the oscillator strength involves the charge-transfer character of the lower two

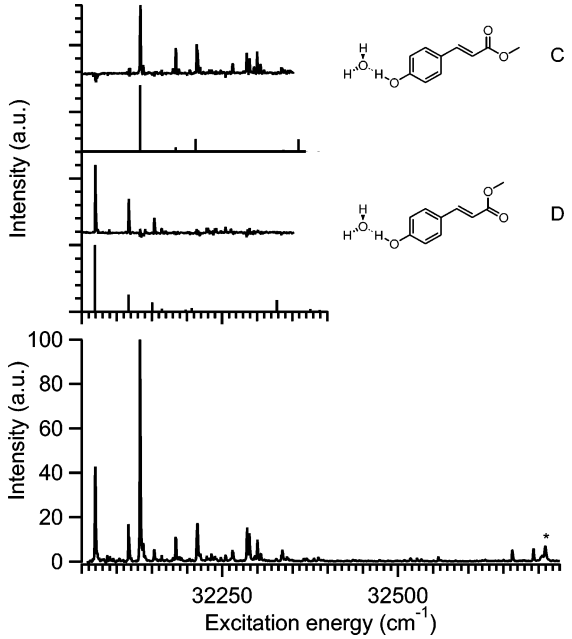

Figure 5. Bottom: LIF excitation spectrum of the OMpCA(H_2O) complex. Top: hole-burning spectra of the two conformers s-cis (C) and s-trans (D) (solid lines) and the Franck−Condon simulations for both conformers (stick spectra). The hole-burning laser was fixed at 32133 and 32069 cm^{-1} for the spectra of C and D conformers, respectively.

excited singlet states of OMpCA. The S_2 state has a larger charge-transfer character than the S_1 state.[7,8] Complexation with water will therefore change the energy gap between the two states and lead to an increased mixing (or possibly even reversal) of the two states. Since the $S_0 \leftrightarrow S_2$ transition has a considerably larger oscillator strength than the $S_0 \leftrightarrow S_1$ transition, this would enhance the intensity of the latter transition. EOM-CCSD calculations of the energies and oscillator strengths of the vertical transitions in the complex are listed in Table 1. Indeed, there is an increase (by a factor 2) of the calculated oscillator strength for the $S_0 \leftrightarrow S_1$ transition. The weight of the HOMO→LUMO configuration rises in the S_1 state and drops in the S_2 state, consistent with an increase in V′/V mixing. The S_1-S_2 gap, however, is not much reduced, which can be taken as evidence that the mixing (the coupling of these states) is very strong and not "linear" in energy. We also note that it is sensitive to the basis set: the calculated oscillator strength for the $S_0 \leftrightarrow S_1$ transition of pCA changes from 0.06 with the 6-31G* basis used in ref 8 to 0.16 with the 6-31+G* basis of the current calculations. The above-mentioned 2 fold increase in the oscillator strength does not, however, completely account for the intensity rise (more than 10 times) that occurs upon complexation with water. Obviously, there is another factor behind this, with the most probable one being a decrease in the nonradiative decay rate. The latter, in fact, is in line with the dramatic reduction that occurs in the nonradiative decay rate of phenol in its first excited singlet state upon complexation with water.[38] The current explanation for this reduction has been proposed by Sobolewski and Domcke[34,35] and is based on the removal of a conical intersection between the Rydberg-like $\pi\sigma^*$ state and the ground state on complexation with water. This $\pi\sigma^*$ state is dissociative along the OH stretch coordinate in bare phenol, leading to a conical intersection with the ground state and thus providing a route for rapid depopulation of the S_1 state. In the water complex, however, the $\pi\sigma^*$ is destabilized at larger phenolic O−H distances, which leads to a shallow minimum and an absence of the conical intersection. Because of the similarity of phenol and OMpCA, it seems likely that the same $\pi\sigma^*$ state plays an analogous role in OMpCA. In line with this similarity, our EOM-CCSD calculations predict that the $\pi\sigma^*$ state undergoes an increase in its vertical excitation energy upon complexation with water (Table 1). While it is not large (0.15 eV), in combination with the decrease in energy for both $\pi\pi^*$ states, it will lead to raising of the energy of the conical intersection between the $\pi\pi^*$ and $\pi\sigma^*$ states. The latter can be an additional reason of a smaller decay rate, revealed in the water cluster. The conclusion that the $\pi\sigma^*$ state is important to understand the decay of the S_1 state of OMpCA is relevant, as it implies that its effects should also be taken into account in studies that relate excited-state lifetimes of pCA-like chromophores in solution to trans-to-cis isomerization.[39]

TABLE 2: Experimental and TD-DFT Calculated Frequencies (cm^{-1}) of the Inter- and Intramolecular Modes of OMpCA(H_2O)

	S_0		S_1		
conformer	expt	calcn	expt	calcn	assignment
C	44	43	50	50	β_1
	80	75	81	79	a'_1
	143	157	155−175	157	σ?
D		43	48	48	β_1
	80	79	84	81	a'_1
	145	165	150−175	169	σ?

As is the case for the bare molecule, the excitation spectrum of the water complex contains contributions from several conformations as indicated by the hole-burning spectra displayed in Figure 5. Because we expect only a very small effect of the orientation of the OH group on the spectrum, we conclude that the origins at 32069 and 32133 cm^{-1} must come from the s-trans (D) and s-cis (C) conformers, respectively, and that we see only one of the OH syn or anti conformations.[40] This is in first instance rather unexpected. However, above we have concluded that the observed intensity distribution over the s-cis and s-trans conformers gives evidence for a lowering of the barrier for interconversion. The apparent absence of signals from either the syn or anti conformation could thus indicate an even further lowering of this barrier upon complexation with water.

TD-DFT-based Franck−Condon simulations of structures C and D appear as stick spectra in Figure 5 below the corresponding hole-burning spectra. The agreement between experiment and simulation is very good. The most intense vibrational bands in both spectra can easily be assigned on the basis of the simulations (see Table 2). The intermolecular in-plane bending mode (β_1 in the nomenclature of Schütz et al.[41]) is found at a frequency of 47 cm^{-1} in C and 51 cm^{-1} in D. Similar to A and B, the a'_1 mode is also present in the spectra of C and D at 84 and 81 cm^{-1}, respectively.

Although the limited signal strength makes it difficult to obtain high-resolution dispersed emission spectra with a good signal-to-noise ratio, some information on the ground state vibrational frequencies can be obtained from the spectra shown in Figure 6. The assignments are listed in Table 2. The inter- and intramolecular bending modes β_1 and a'_1 are easily recognized. For both conformers the frequency of the intermolecular bending mode is slightly lower in the ground state than in the excited state. This is expected because of the much stronger hydrogen bond in the excited state.[37] A similar shift to higher frequency in the excited-state can be expected for the intermolecular stretching mode σ (for phenol $\sigma'' = 151$ cm^{-1} and $\sigma' = 156$ cm^{-1} [42]). We tentatively assign the peak at 143 cm^{-1} in C and 145 cm^{-1} in D to σ'. The σ'' should then be assigned to one of the group of peaks appearing between 155 and 175 cm^{-1} in C and 150−175 cm^{-1} in D.

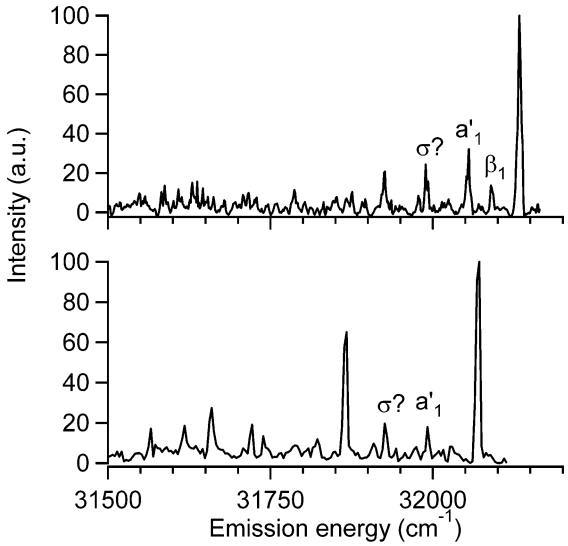

Figure 6. Emission spectra of OMpCA(H_2O). Top: s-cis conformer C. Bottom: s-trans conformer D.

A final remark concerns the two intense resonances that are observed at 32663 and 32693 cm^{-1} in Figure 5, close to the origin of the bare molecule. The intensities of these bands depend sensitively on the backing pressure and valve timings, they do not display dips with the hole-burning laser set at either one of the AI, AII, B, C, or D origins, and they do not show up in the MR-REMPI spectra of the bare molecule or the water cluster. It is therefore likely that they derive from OMpCA-$(H_2O)_n$ clusters with $n > 1$, but at this moment we do not have enough information to make a definite assignment.

Conclusions

The present work on OMpCA, the methyloxy ester of *p*-coumaric acid, has provided the first high-resolution spectroscopic study of the lower excited singlet states of the neutral form of the PYP chromophore in the gas phase. Using hole-burning spectroscopy, we have shown that the excitation spectra contain contributions from four conformations that differ in their orientation of the phenolic OH group and the stereochemistry of the C_8-C_9 single bond. Comparison with analogous spectra of the related *p*-vinylphenol molecule suggests that the carboxylic ester group lowers the barrier associated with the interconversion between the syn and anti OH conformers in the electronic ground state.

In combination with TD-DFT calculations of vibrational activity in the excitation and emission spectra of the lower excited singlet states, it has been concluded that the carboxylic ester group does not influence the relative energies and properties of the lower excited states in the Franck−Condon region significantly. Analogous to the situation in pVP, and in agreement with the results from EOM-CCSD calculations, the S_1 state only has a minor contribution from the HOMO → LUMO configuration, and the $S_0 \leftrightarrow S_1$ transition has a small oscillator strength. The equilibrium geometry of this state is rather similar to that of the ground state, and the excitation spectrum consequently shows limited vibrational activity. The S_2 state, in contrast, has a dominant contribution from the HOMO → LUMO configuration, the $S_0 \leftrightarrow S_2$ excitation has a larger oscillator strength, and excitation to S_2 is accompanied by larger geometry changes and more vibrational activity in the spectrum.

Complexation of OMpCA with a single water molecule changes the excitation spectrum of the chromophore considerably. It causes an unexpected large red shift (641 cm^{-1}) but, even more intriguing, leads to a large increase of the laser-induced fluorescence signal. We have not yet been able to conclusively identify the mechanism responsible for this increase, but the available experimental and theoretical material suggests that it might be due to (i) increasing the oscillator strength of the lowest $\pi\pi^*$ transitions as well as (ii) stabilization of the $\pi\pi^*$ states and destabilization of the $\pi\sigma^*$ state, which provides in phenol an efficient pathway for nonradiative decay. The interaction with water raises the energy of a conical intersection between the $\pi\pi^*$ and $\pi\sigma^*$ states and removes a conical intersection between the $\pi\sigma^*$ and ground state, both of which can give rise to a decrease in the nonradiative decay rate.

Acknowledgment. This work has been supported by The Netherlands Organization for Scientific Research (NWO). Financial support by a DFG/CNRS collaboration project is gratefully acknowledged. E.V.G. cordially appreciates a Heidelberg Graduate School fellowship.

References and Notes

(1) Hellingwerf, K. J.; Hendriks, J.; Gensch, T. *J. Phys. Chem. A* **2003**, *107*, 1082.
(2) Lee, I.; Lee, W.; Zewail, A. H. *Proc. Natl. Acad. Sci.* **2006**, *103*, 258.
(3) Nielsen, I. B.; Boyé-Péronne, S.; El Ghazaly, M. O. A.; Kristensen, M. B.; Nielsen, S. B.; Andersen, L. H. *Biophys. J.* **2005**, *89*, 2597.
(4) Ryan, W. L.; Gordon, D. J.; Levy, D. H. *J. Am. Chem. Soc.* **2002**, *124*, 6194.
(5) Kort, R.; Vonk, H.; Xu, X.; Hoff, W. D.; Crielaard, W.; Hellingwerf, K. J. *FEBS Lett.* **1996**, *382*, 73.
(6) de Groot, M.; Buma, W. J. *J. Phys. Chem. A* **2005**, *109*, 6135.
(7) de Groot, M.; Buma, W. J.; Gromov, E. V.; Burghardt, I.; Köppel, H.; Cederbaum, L. S. *J. Chem. Phys.* **2006**, *125*, 204303.
(8) Gromov, E. V.; Burghardt, I.; Köppel, H.; Cederbaum, L. S. *J. Phys. Chem. A* **2005**, *109*, 4623.
(9) Interestingly, our calculations on the methylthio ester of pCA (unpublished results) predict that this species is unstable in the lowest $\pi\pi^*$ state, undergoing abstraction of the SCH_3 fragment. The latter is, however, not the case for *p*-coumaric thioacid.
(10) Gromov, E. V.; Burghardt, I.; Köppel, H.; Hynes, J. T.; Cederbaum, L. S. *J. Photochem. Photobiol. A* **2007**, *190*, 241.
(11) Ko, C.; Levine, B.; Toniolo, A.; Manohar, L.; Olsen, S.; Werner, H.; Martínez, T. J. *J. Am. Chem. Soc.* **2003**, *125*, 12710.
(12) Levine, B. G.; Ko, C.; Quenneville, J.; Martínez, T. J. *Mol. Phys.* **2006**, *104*, 1039.
(13) Rijkenberg, R. A.; Bebelaar, D.; Buma, W. J.; Hofstraat, J. W. *J. Phys. Chem. A* **2002**, *106*, 2446.
(14) Treutler, O.; Ahlrichs, R. *J. Chem. Phys.* **1995**, *102*, 346.
(15) Von, Arnim, M.; Ahlrichs, R. *J. Comp. Chem.* **1998**, *19*, 1746.
(16) Deglmann, P.; Furche, F. *J. Chem. Phys.* **2002**, *117*, 9535.
(17) Deglmann, P.; Furche, F.; Ahlrichs, R. *Chem. Phys. Lett.* **2002**, *362*, 511.
(18) De Groot, M.; Buma, W. J. *Chem. Phys. Lett.* **2007**, *435*, 224.
(19) De Groot, M.; Buma, W. J. *Chem. Phys. Lett.* **2006**, *420*, 459.
(20) Perdew, J. P. *Phys. Rev. B* **1986**, *33*, 8822.
(21) Becke, A. D. *Phys. Rev. A* **1988**, *38*, 3098.
(22) Becke, A. D. *J. Chem. Phys.* **1993**, *98*, 5648.
(23) Lee, C.; Yang, W.; Parr, R. G. *Phys. Rev. B* **1988**, *37*, 785.
(24) Becke, A. D. *J. Chem. Phys.* **1993**, *98*, 1372.
(25) Scott, A. P.; Radom, L. *J. Phys. Chem.* **1996**, *100*, 16502.
(26) Buma, W. J.; Zerbetto, F. *J. Chem. Phys.* **1995**, *103*, 10492.
(27) Doktorov, E. V.; Malkin, I. A.; Man'ko, A. V. I. *J. Mol. Spectrosc.* **1977**, *64*, 302.
(28) Zwier, J. M.; Wiering, P. G.; Brouwer, A. M.; Bebelaar, D.; Buma, W. J. *J. Am. Chem. Soc.* **1997**, *119*, 11523.
(29) GAMESS version, June 27, 2005 (R2).
(30) Schmidt, M. W.; Baldridge, K. K.; Boatz, J. A.; Elbert, S. T.; Gordon, M. S.; Jensen, J. H.; Koseki, S.; Matsunaga, N.; Nguyen, K. A.; Su, S.; Windus, T. L.; Dupuis, M.; Montgomery Jr, J. A. *J. Comput. Chem.* **1993**, *14*, 1347.
(31) Sekino, H.; Bartlett, R. J. *Int. J. Quantum Chem., Quantum Chem. Symp.* **1984**, *18*, 255.
(32) Werner, H.-J.; Knowles, P. J.; Lindh, R.; Manby, F. R.; Schütz, M.; Celani, P.; Korona, T.; Rauhut, G.; Amos, R. D.; Bernhardsson, A.; Berning, A.; Cooper, D. L.; Deegan, M. J. O.; Dobbyn, A. J.; Eckert, F.; Hampel, C.; Hetzer, G.; Lloyd, A.W.; McNicholas, S. J.; Meyer, W.; Mura,

M. E.; Nicklass, A.; Palmieri, P.; Pitzer, R.; Schumann, U.; Stoll, H.; Stone, A. J.; Tarroni, R.; Thorsteinsson, T. MOLPRO, version 2006.1, a package of ab initio programs; see http://www.molpro.net.

(33) It has been suggested[39] that the difference in radiative lifetime between the neutral and deprotonated (anionic) form of the OMpCA in solution should be attributed to the coupling of the nπ* state with a nearby $\pi\pi$* state. Our current and previous[10] calculations, however, imply that the complete explanation involves the switching of the V′ and V states upon deprotonation.

(34) Sobolewski, A. L.; Domcke, W. *J. Phys. Chem. A* **2001**, *105*, 9275.

(35) Sobolewski, A. L.; Domcke, W.; Dedonder-Lardeux, C.; Jouvet, C. *Phys. Chem. Chem. Phys.* **2002**, *4*, 1093.

(36) A note about orientation of the water molecule: The water hydrogens lie above and below the molecular plane of OMpCA, being oriented "anti" to the chromophore with respect to O−H−O line. C_s symmetry of the bare chromophore is preserved.

(37) Zwier, T. S. *Annu. Rev. Phys. Chem*. **1996**, *47*, 205.

(38) Sur, A.; Johnson, P. M. *J. Chem. Phys*. **1986**, *84*, 1206.

(39) Espagne, A.; Paik, D. H.; Changenet-Barret, P.; Martin, M. M.; Zewail, A. H. *ChemPhysChem* **2006**, *7*, 1717.

(40) An alternative explanation is that the bands of the two conformations exactly superimpose. It would be hard to believe that this would occur for every single band, and this explanation is therefore rejected.

(41) Schuetz, M.; Buergi, T.; Leutwyler, S.; Fischer, T. *J. Chem. Phys*. **1993**, *98*, 3763.

(42) Stanley, R. J.; Castleman, A. W.; Jr. *J. Chem. Phys*. **1991**, *94*, 7744.